



Catalytically active nano-porous cobalt-palladium alloys

Shay Avisar^a, Yahel Shner^a, Raed Abu-Reziq^a, Inna Popov^b, Avi Bino^{a,*}

^a Institute of Chemistry, The Hebrew University of Jerusalem, The Edmond J. Safra Campus, Givat Ram, 9190401 Jerusalem, Israel

^b The Center for Nanoscience and Nanotechnology, The Hebrew University of Jerusalem, The Edmond J. Safra Campus, Givat Ram, 9190401 Jerusalem, Israel



ARTICLE INFO

Article history:

Received 23 May 2021

Received in revised form 12 August 2021

Accepted 7 September 2021

Available online 12 September 2021

Keywords:

Transition metal alloys and compounds

Gas-solid reactions

Catalysis

Vacancy formation

Scanning electron microscopy (SEM)

X-ray diffraction

ABSTRACT

The potential advantages of nano-alloys and particularly, nano-porous alloys, place them at the "spotlight" of heterogeneous catalysis. Nevertheless, controlling the precise compositions of these materials is still a synthetic challenge. Previous research introduced the fabrication of metals and alloys with a high nano-scale porosity and controllable compositions, via a hydrogen-mediated chemical reduction process of metal complex salts. We have used this procedure to obtain two magnetic nano-porous Co-Pd alloys, pure porous palladium and pure porous cobalt. Single crystal X-ray diffraction studies enabled structural determination of the two Co-Pd bi-complex salts that were used as precursors for these alloys. Powder X-ray diffraction studies determined the crystalline phases of the alloys and indicated the nanometric size of their crystallites. High-resolution scanning electron microscopy indicated that these alloys assemble as highly porous clusters of interconnected nano-crystallites. It also indicated that each alloy cluster preserves the micro-metric morphologies of its salt precursor. Energy dispersive X-ray spectroscopy showed that the alloys exhibit uniform composition down to the micro-level, which preserved the Co/Pd ratio within the salts. Focused ion beam tomography enabled 3D structural representation of the alloys and metals. Geometrical analysis of the 3D reconstructed data determined 90% porosity and a specific surface area of $\sim 100 \text{ m}^2/\text{g}$ for the alloys. In addition, the alloys showed improved catalytic activity in the semi-hydrogenation of phenylacetylene, compared to the pure metals and commercial Pd/C. Moreover, their magnetic properties enabled facile recovery at the end of the reaction. The yield for styrene in this reaction was increased using "design of experiments" (DOE), a method for optimization of reaction conditions. Furthermore, our experiments implied that a highly porous structure significantly improves the selectivity of styrene in the reaction. These results demonstrated the advantage of fabricating nano-porous alloys with uniform compositions that may exhibit special properties and serve as new and efficient catalysts.

© 2021 Elsevier B.V. All rights reserved.

1. Introduction

Multi-element nano-dimensional and nano-porous metallic materials are capable of combining synergistic properties of alloys and nanoscale matter such as high surface area. Therefore, these materials attract considerable attention in several fields including heterogeneous catalysis. Many techniques have been developed for the synthesis of nano-alloys in the gas-phase, in solution, as a supported phase on a substrate, or in a matrix [1,2].

Destructive techniques such as de-alloying [3,4] or galvanic displacement [5,6] produce metallic materials with nano-scale porosity. However, these techniques restrict composition control and often produce structures with diverse compositions [7–12]. Consequently,

examples of alloys with nanoscale porosity and controllable composition are still rare.

A different preparative approach has demonstrated the preparation of numerous alloys with nano-scale porosity through the chemical reduction of metal complex salts [13–18]. These metallic materials assemble as highly porous ($\sim 90\%$ porosity) nanoparticle clusters that preserve the morphologies and volumes of their microcrystalline salt precursors. In addition, they preserve the precise stoichiometric ratio between the two different metal atoms that exist in the bi-complex salt precursors and exhibit a uniform spatial composition down to the sub-micro-level. Some studies have also shown examples of the catalytic reactivity of these alloys [19–22]. Yet, there is only little knowledge about the correlation between the structure of these types of alloys and their catalytic reactivity.

Correlating between structure and reactivity of catalysts in a reaction requires information about the conditions of the reaction in which each catalyst operates such as the temperature or the reaction

* Corresponding author.

E-mail address: bino@mail.huji.ac.il (A. Bino).

period. A better comparison also requires the optimized conditions for each catalyst. OVAT ("one variable at a time") is the traditional approach for this kind of optimization. Nevertheless, this approach often does not lead to the real optimum and is only valid if there is no interaction between the variables. Moreover, OVAT approach requires many experiments for gaining a small amount of information regarding the investigated system. An alternative statistical method – DOE ("design of experiments"), also noted as "experimental design", enables collection of precise information from fewer experiments. Particularly, DOE enables to consider the effect of the interaction between the variables upon the reaction results [23]. Consequently, this approach has recently gained some popularity as an optimization method, including in heterogeneous catalysis [24–29].

Herein we utilize chemical reduction processes, mentioned above, in order to produce two cobalt–palladium alloys, pure cobalt, and pure palladium with nano-scale porosity. The catalytic reactivity of these alloys was examined using the semi-hydrogenation of phenyl-acetylene as a model reaction. A specific focus was directed towards conversion, selectivity, and yield of styrene. DOE method was applied to optimize the conditions of the reaction for each alloy catalyst, including hydrogen pressure, temperature, and reaction periods. Next, the reactivity of these alloys were compared with each other, with the pure metals and with commercial Pd/C. Finally, a specific focus was directed at the correlation between these materials structures and compositions and their catalytic reactivity.

2. Materials and methods

a. Bi-complex salts (BCS) preparation

Microcrystalline bi-complex metal salts (BCS) $[\text{Co}(\text{NH}_3)_6]_2[\text{PdCl}_4]_3 \cdot 8\text{H}_2\text{O}$ (**1**) and $[\text{Co}(\text{NH}_3)_5\text{Cl}][\text{PdCl}_4]$ (**2**) were synthesized in a similar manner. Mixing concentrated cold (cooled in an ice bath) aqueous solutions (about 20 mg/mL) of $[\text{Co}(\text{NH}_3)_6]\text{Cl}_3$ and $(\text{NH}_4)_2[\text{PdCl}_4]$ in a molar ratio of 2:3 respectively, yielded a precipitation of the brown-orange salt **1**. The precipitate was separated, washed three times with deionized cold water, and left to dry in the open air. Mixing concentrated aqueous solutions (about 10 mg/mL) of $[\text{Co}(\text{NH}_3)_5\text{Cl}]\text{Cl}_2$ and $\text{K}_2[\text{PdCl}_4]$ in a molar ratio of 1:1 led to the formation of a reddish powder of **2**. The precipitate was separated, washed three times with deionized water, one time with acetone, and left to dry in the open air. Single crystals of **1** and **2** were also prepared using membrane diffusion technique.

b. Preparation of metals and alloys

All metallic materials were prepared according to a previously published procedure [16]. Co–Pd alloys were prepared by chemical reduction of salt **1** and salt **2** in a tube furnace under a flow of 1 atm H_2 –Ar mixture (5%/95%) at 200 °C for 24 h. Porous palladium and cobalt were prepared by reduction of $\text{K}_2[\text{PdCl}_4]$ and $[\text{Co}(\text{NH}_3)_5\text{Cl}]\text{Cl}_2$, respectively, in a tube furnace under a flow of 1 atm H_2 –Ar mixture (5%/95%) at 350 °C for 24 h. The resulting black powders of metals or alloys were cooled to room temperature and kept under a stream of Ar for additional 10 min

c. Single-crystal X-ray diffraction (SC-XRD) analysis

Single crystals of BCS **1** and **2** were transferred to a Bruker SMART APEX CCD X-ray diffractometer equipped with a graphite monochromator. The system was controlled by a pentium-based PC running the SMART software package [30]. Data were collected at room temperature using $\text{Mo K}\alpha$ radiation ($\lambda = 0.71073 \text{ \AA}$). The raw data frames were transferred to a second PC computer for integration and reduction by the SAINT program package [31]. The structures were

solved and refined by the SHELXTL software package [32]. These data can be obtained free of charge from The Cambridge Crystallographic Data Centre at <https://www.ccdc.cam.ac.uk/structures/>. Further details of the crystal structures may be obtained from the Fachinformationszentrum Karlsruhe, 76344 Eggenstein-Leopoldshafen (Germany), on quoting the depository numbers CSD-2026589, 2026590.

d. Powder X-ray diffraction (PXRD) analysis

Powder X-ray diffraction patterns were measured using a Philips PW1820 diffractometer with a Philips PW1710 proportional detector. The measurements were carried out using $\text{Cu K}\alpha$ ($\text{K}\alpha_1 \lambda = 1.54060 \text{ \AA}$, $\text{K}\alpha_2 \lambda = 1.54439 \text{ \AA}$) X-ray source. The Cu tube was operated at a voltage of 40 kV and a current of 30 mA. XRD measurements were recorded in Bragg–Brentano reflection geometry. The scan was performed in the 2θ ranges of 10–60° for BCS and 30–90° for metals and alloys, with a step width of 0.02° and a step time of 1 s

e. Electron microscopy

High-resolution scanning electron microscopy (HR-SEM) and energy dispersive x-ray spectroscopy (EDS) measurements were conducted using an FEI Sirion HR-SEM equipped with EDAX EDS and FEI Magellan 400 L XHR-SEM equipped with an Oxford Instruments XMAX SDD EDS working on an INCA450 platform.

f. FIB tomography

3D structure of nano-porous alloys and metals prepared in this work was studied with Focused Ion Beam (FIB) tomography. Milling and data collection was done at FEI Dual beam FIB Helios 460 F Lite equipped with Auto Slice & View software. Reconstruction of experimental data and geometrical analysis of 3D reconstructed volume was performed with FEI AVIZO 9.2 software.

g. Catalytic studies

Catalytic reactions were performed in a 50 mL stainless steel high-pressure reactor (Parr Instruments). In a typical reaction, 2.5 mg of the catalyst powder (Co–Pd alloy, Co metal, Pd metal or Sigma Aldrich Pd/C 10% wt.) and 500:1 mol/mol ratio of phenylacetylene/catalyst were dissolved in 1–2 mL of chloroform-D in a 4 mL glass vessel. The vessel was inserted to a larger 50 mL glass vessel that was placed in the reactor. The reactor was purged three times with 10 bar of H_2 (99.999%) prior to the reaction. Hydrogen pressure and temperature of the reactor were adjusted (as described in Table 2 and Table 3 in section 3.2 below), and the reaction vessel was kept with constant stirring under these conditions (pressure & temperature) for 1–4 h. Following the reaction, fractions of the reaction mixture were extracted, diluted with chloroform-D and separately analyzed by GC-MS (Fisher-Scientific) and ^1H NMR (Bruker).

3. Results and discussion

a. Preparation and characterization of bi-complex salts (BCS), nano-porous alloys and porous metals

Two Co–Pd BCS, their corresponding alloys, and pure cobalt and palladium metals were prepared through modifications of a previously published procedure [16]. The two Co–Pd bi-complex salts $[\text{Co}(\text{NH}_3)_6]_2[\text{PdCl}_4]_3 \cdot 8\text{H}_2\text{O}$ (**1**) and $[\text{Co}(\text{NH}_3)_5\text{Cl}][\text{PdCl}_4]$ (**2**) were prepared by mixing concentrated aqueous solutions of counter-charged cobalt and palladium complexes as described in Eqs. (1a) and (1b), respectively:

Table 1

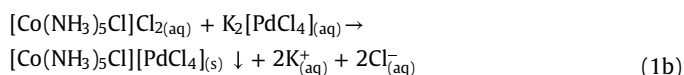
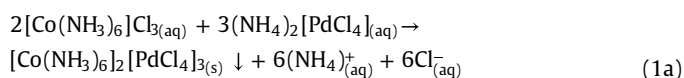
Values of porosity and specific surface area of Co-Pd alloys, pure palladium, and pure cobalt.

Metallic material	Porosity (%)	Specific surface area (m ² /g)
Co ₂ Pd ₃	90	109
CoPd	90	99
Pd	90	50
Co	22	5

Table 2

The levels of the variables for the DOE.

Variable	H ₂ Pressure (psi)	Temperature (°C)	Reaction time (h)
Minimum level (-1)	40	25	1
Maximum level (+1)	300	40	4



Single crystals of these salts were also prepared and structurally characterized using X-Ray crystallography. Earlier studies already reported the characterization of salt 2 using powder diffraction [13], yet we have crystallized and determined its structure using single-crystal X-ray crystallography for the first time. The unit cell of each of the mentioned crystals comprises cobalt and palladium atoms in a specific ratio – 2:3 for salt 1 and 1:1 for salt 2 (Fig. 1). These ratios

Table 3

The set of eight DOE experiments, and their responses for: (a) Co₂Pd₃ catalyst, and (b) CoPd catalyst.

Experiment number	H ₂ pressure (psi)	Temperature (°C)	Reaction time (h)	Conversion of phenylacetylene (%)	Styrene's selectivity (%)	Styrene's yield (%)
3a. Co ₂ Pd ₃ catalyst						
1	300	40	4	100	1	1
2	40	40	4	88	92	81
3	300	25	4	100	13	13
4	40	25	4	49	93	46
5	300	40	1	100	70	70
6	40	40	1	31	94	29
7	300	25	1	61	95	58
8	40	25	1	21	93	20
3b. CoPd catalyst						
1	300	40	4	100	0	0
2	40	40	4	97	88	85
3	300	25	4	100	0	0
4	40	25	4	65	91	59
5	300	40	1	100	75	75
6	40	40	1	39	92	36
7	300	25	1	100	20	20
8	40	25	1	12	92	11

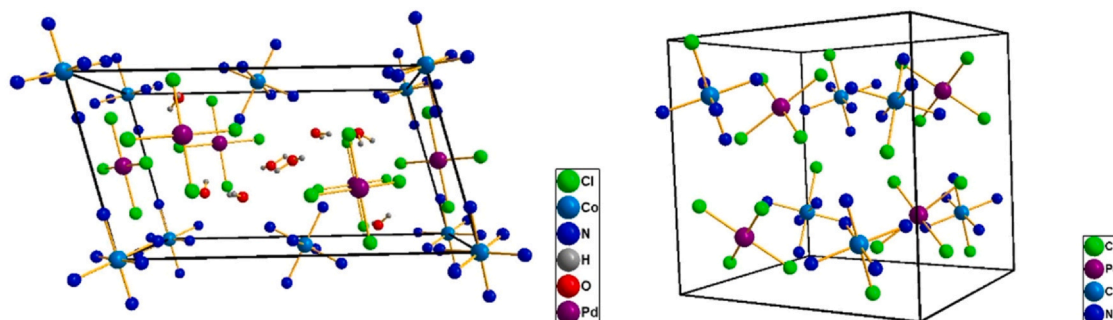
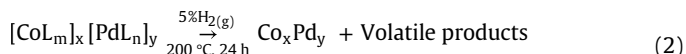


Fig. 1. The unit cells of the single crystals: (a) [Co(NH₃)₆]₂[PdCl₄]₃·8H₂O, and (b) [Co(NH₃)₅Cl][PdCl₄]. The hydrogen atoms of the ammonia ligands were omitted for clarity.

resulted from the various electrostatic interactions between the two counter-charged cobalt and palladium complexes.

PXRD analysis of the BCS (Fig. S1) demonstrates high correspondence between the experimental and simulated patterns, thus indicating the purity and the ordered structure of the micro-crystalline BCS samples.

Thermal treatment of the BCS 1 and 2 under a reducing environment (1 atm flow of 5% H₂ in 95% Ar, 200 °C) for 24 h resulted in formation of the corresponding highly porous alloys Co₂Pd₃ and CoPd, respectively, as described in Eq. (2):



Application of a similar reduction process to [Pd(NH₃)₄]Cl₂ and [Co(NH₃)₅Cl]Cl₂ provided pure Pd and Co porous metals respectively (Fig. S2).

PXRD analysis of the alloys indicated that they were crystalline and composed of two phases. Fig. 2 shows that the major crystalline phase in both samples is isostructural to the fcc Pd (JCPDF # 04-015-0492). The second crystalline phase presented in the samples appeared as an isostructural to the hcp Co (JCPDF # 01-089-7373). A systematic shift of the diffraction peaks indicates formation of solid solutions in both structures. The estimated size of the crystallites calculated with Scherrer formula was a few nanometers in the hcp Co-like phase and in the range of tens of nanometers in the fcc Pd-like phase (Table S1). The phase content of each alloy was only qualitatively estimated, due to the large FWHM (full width of half-maximum) and low intensity of the diffraction peaks of Co-based phase. This estimation revealed that the amount of Pd-like phase was higher in Pd-rich Co₂Pd₃ sample, while the amount of Co-like phase was higher in Co-rich CoPd sample.

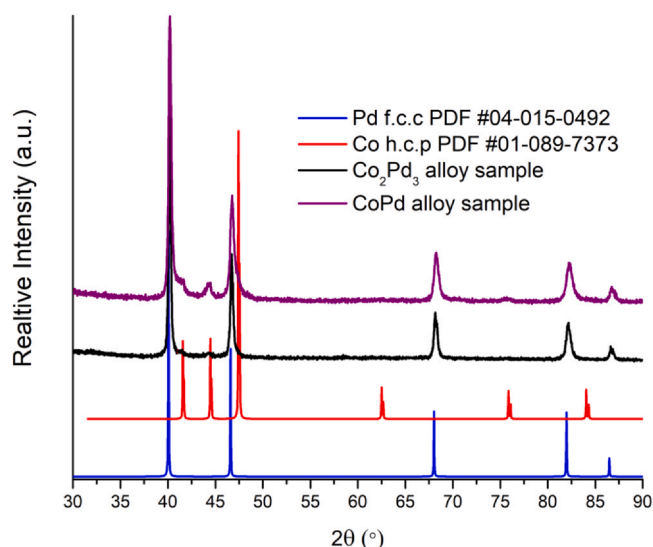


Fig. 2. Comparisons of powder diffractions of Co-Pd nano-porous alloys to the ICDD database.

The equilibrium phase diagram for Co-Pd system predicts a single fcc – based solid solution phase for the binary compositions prepared in this work (60/40 and 50/50 at. ratio of Pd/Co) below 200 °C [33]. Therefore, we assumed that both Co-Pd alloys obtained in this work were metastable two-phase bimetallic alloys composed of nano-crystalline solid-solution phases. This assumption was further probed via direct identification of the elemental composition in the BCS and the corresponding alloys.

Fig. 3 demonstrates a very good agreement between the average Pd/Co ratio in BCS **1** and **2** and their corresponding alloys, considering the statistical errors of the EDS results. It also shows a similar agreement between the Pd/Co ratios directly measured by EDS and calculated from the data of SC-XRD. These results indicated that the initial Pd/Co ratio of the crystalline BCS was preserved almost perfectly at the reduction. Therefore, we concluded that the reduced alloys are indeed composed of two nano-crystalline solid solution phases. We assumed that the preservation of Pd/Co ratio during the reduction was provided by relatively low diffusion rates induced by

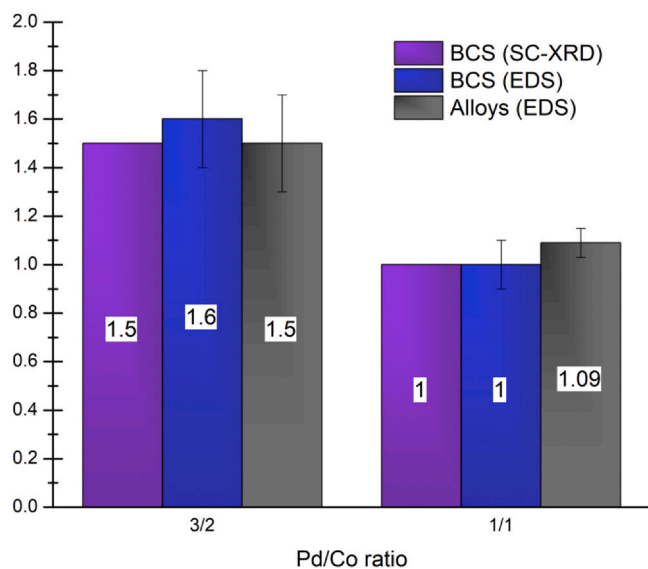


Fig. 3. A comparison between: the Pd:Co ratios in the BCS calculated using SC-XRD data, the Pd:Co average ratios in the BCS determined using EDS, and the Pd:Co average ratios in the Co-Pd alloys determined using EDS.

the relatively low reduction temperature. This is since at elevated temperatures, the metal atoms have rather high diffusion rates that prevent typical metallurgical processes from manufacturing nano-dimensional metals and alloys [34,35].

Fig. 4 shows that the morphologies and the volumes of the BCS micro-crystallites were almost perfectly preserved in the alloys during the reduction process, yet the initially smooth faces of micro-particles (4a, 4c) became porous (4b, 4d). HR-SEM images of porous palladium and cobalt metals, prepared using the same process, have shown similar results (Fig. S3, Fig. S4). Nevertheless, while the structure of the porous Co-Pd alloys and palladium were more alike, cobalt acquired a coarser and a less porous structure (Fig. S3).

HR-SEM imaging shown in Fig. 5 reveals that the reduced alloys acquired a highly porous structure of interconnected nano-dimensional metal ligaments separated by the pores of the similar size, as already known for this process [16]. Besides, the dimension of these ligaments was very similar to the crystal size estimated from the PXRD data (Table S1), i.e., the final metal network was nano-dimensional, nanocrystalline and nano-porous. This specific structure was certainly obtained during the reduction process at which all ligands and solvent molecules evaporated leaving only metallic material behind, as already shown earlier [16].

3D reconstruction of the reduced alloys volume using FIB tomography shown in Fig. 6 had further confirmed their nano-porous structure. 3D reconstruction of pure palladium and pure cobalt metals revealed that the former had acquired a highly nano-porous structure, while the latter has acquired a coarser and a less porous structure (Fig. S6).

Geometrical analysis of the 3D reconstructed data of the alloys and metals enabled to determine their porosity and specific surface area (Table 1, Equations S1, S2 and Table S2). Both alloys and pure palladium acquired 90% porosity while pure cobalt acquired only 22% porosity. The specific surface area of the alloys (~100 m²/g) was twice higher than that of pure palladium (50 m²/g), and 20 times higher than that of pure cobalt (5 m²/g). These results agreed with the SEM and XRD observations and indicated the catalytic potential of the alloys, due to their relatively high specific surface areas.

b. Catalytic activity of nano-porous alloys and porous metals

The catalytic activity of the Co-Pd alloys was examined in the semi-hydrogenation of phenyl-acetylene as a model reaction for hydrogenation of alkynes. A specific focus was directed at maximizing conversion and the selectivity towards styrene, as a model of selectivity toward alkenes (see Scheme 1).

GC-MS was used to qualitatively identify the products of the reaction, while 1D ¹H NMR was used to quantitatively determine the conversion and the selectivity of the reactions. The yield of the reaction was calculated by multiplying the conversion and the selectivity for each experiment. The alloys were easily separated at the end of the reactions using a simple magnet, due to their magnetic properties arising from the presence of cobalt atoms. HR-SEM imaging of the alloys after the reaction did not reveal any obvious change in their porous structure (Fig. S7).

Design of experiments (DOE, noted also as experimental design or factorial design) method was used to optimize the conditions for the reactions – including reaction time, temperature, and hydrogen pressure. This technique allowed us to consider the influence of any variable and more important, the influence of the interaction between these variables, upon the conversion, selectivity, and thus yield of the reaction. Each variable had a minimum level and a maximum level, as shown in Table 2, coded as –1 and +1, respectively.

Since there were three variables, eight experiments were performed for each alloy catalyst according to 2^k DOE (where k is the number of variables) model matrix (table S3). Finally, the results of

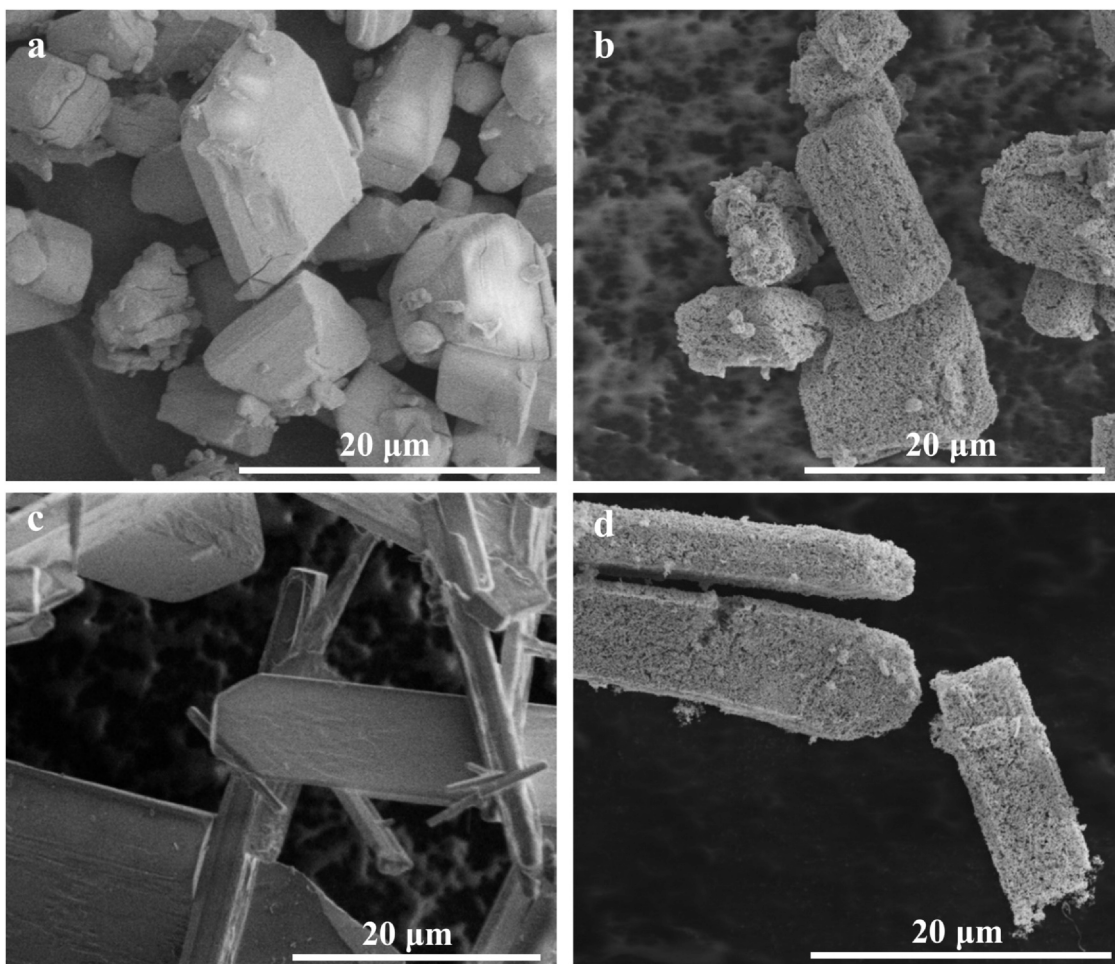


Fig. 4. HR-SEM images of BCS microcrystals and their corresponding nano-porous alloys: (a) salt 1, (b) Co₂Pd₃ alloy, (c) salt 2, (d) CoPd alloy.

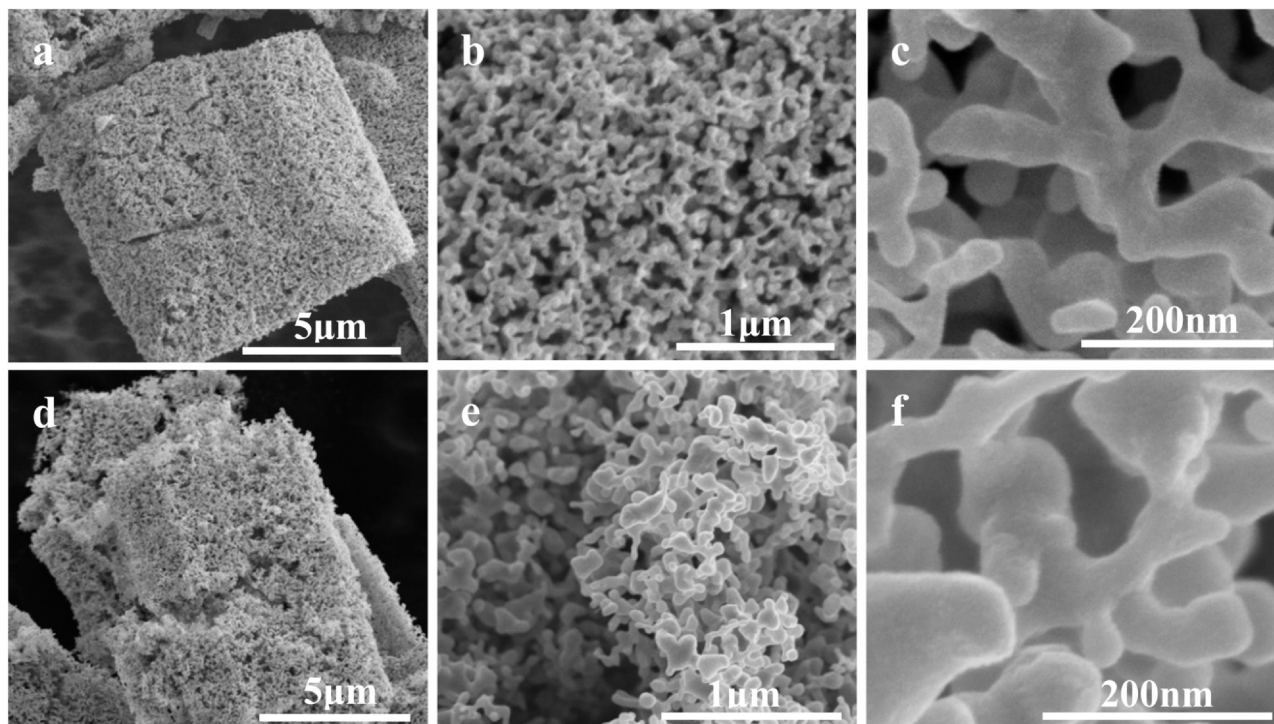


Fig. 5. HR-SEM images acquired under increased magnifications (scale marker bars 5 μm, 1 μm, and 200 nm) at the nano-porous alloys (a)–(c) Co₂Pd₃ and (d)–(f) CoPd.

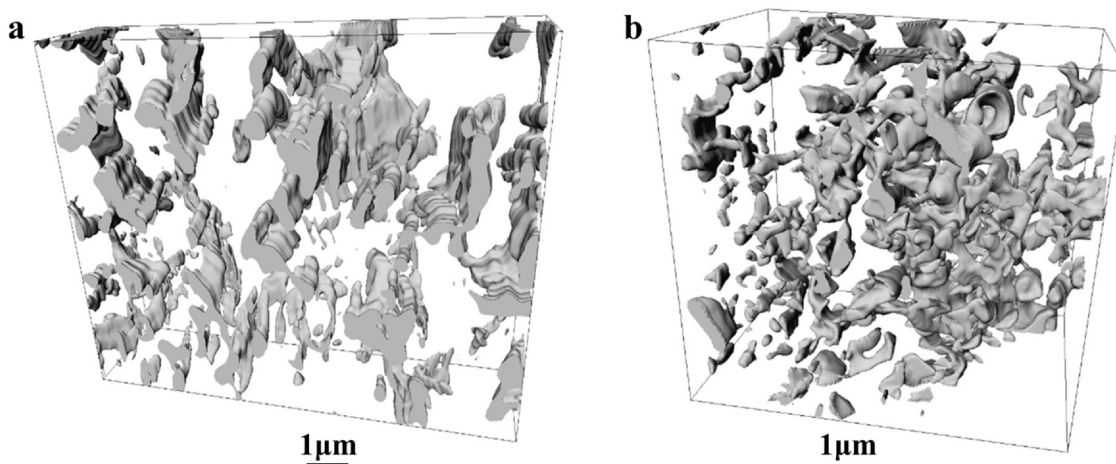


Fig. 6. 3D representations of the nano-porous alloys (a) Co_2Pd_3 and (b) CoPd reconstructed from FIB tomography data.

Table 4

Probing experiments for Co-Pd catalysts.

Catalyst	H_2 pressure (psi)	Temperature ($^\circ\text{C}$)	Time (h)	Conversion of phenylacetylene (%)	Styrene's selectivity (%)	Styrene's yield (%)
Co_2Pd_3	60	35	4	93	97	90
CoPd	60	35	4	99	89	88

these experiments (noted as responses), shown in Table 3, were used to create a "response models" that describes the effects of the mentioned variables on the conversion, selectivity, and yield of the reaction for each catalyst.

According to the mathematical models for Co_2Pd_3 and CoPd catalysts (equations S2-S7), the reaction yield was mostly negatively influenced by the interactions between the hydrogen pressure and time. Namely, if the pressure was increased the time should be decreased (and vice versa) to retain high reaction yield. In addition, both models showed a negative influence of the interaction between the three variables (time, pressure and temperature) on the yield. Therefore, they suggested that setting one of the variables in an opposite direction to the others could help increasing the yield. The models for both catalysts also indicated an increase in the yield by decreasing the pressure and by increasing the temperature. The models did not agree regarding the influences (both their direction and their extent) of the reaction time, the interaction pressure-temperature, and the interaction time-temperature on the yield. Despite that, identical probing experiments were conducted for both catalysts, based on the agreement between the models of the optimized conditions for maximizing the yield. In these experiments, the reaction time was maximized to 4 h, the temperature was set to a high value of 35°C (but not maximized) and the H_2 pressure was set to a relatively low value of 60 PSI although not minimized. The yields achieved in these experiments, as shown in Table 4, mostly agreed with the predications of the models for both catalysts. In fact, this correspondence emphasized the advantage of the DOE method that well predict the influence of variables, and more important, the influence of their interaction, on the examined parameter. Furthermore, the high yields achieved in the probing experiments

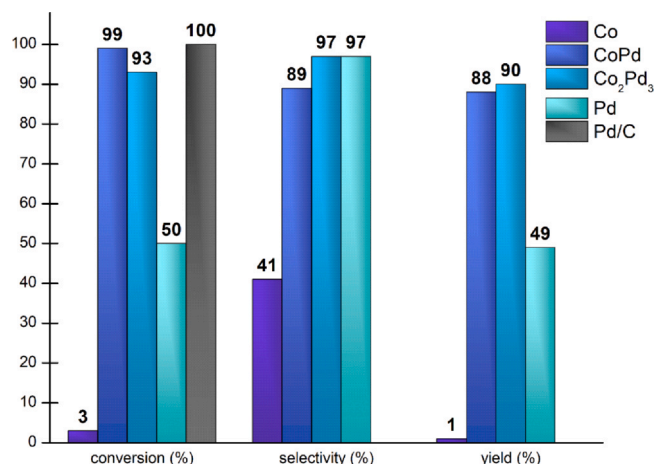
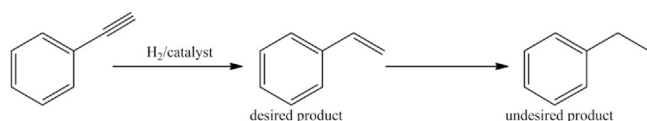


Fig. 7. Comparison between the catalytic activities of Co_2Pd_3 , CoPd , Co , Pd and commercial Pd/C . The selectivity and yield of the reaction with Pd/C were 0% and thus do not appear on the bar chart.

emphasized the importance of DOE method for optimization of catalytic reactions.

The catalytic activity of Co-Pd nano-porous alloy was compared to the activity of cobalt and palladium porous pure metals and commercial Pd/C (10% Pd , sigma) in the optimized conditions mentioned (60 psi H_2 , 35°C , and 4 h). The results, shown in Fig. 7 clearly indicate improvement in the activity of the alloys compared to the pure metals, owing to higher conversions. These results could be attributed to the relatively higher surface area of the alloys compared to the pure metals or to synergistic effects. The results also show that Co-Pd alloys and porous palladium remarkably improved the selectivity of the reaction, hence increasing the yield of styrene, compared to porous cobalt and commercial Pd/C .^a This may imply that the highly porous structure of the alloys and palladium



Scheme 1. Hydrogenation of phenylacetylene reaction.

^a The selectivity and yield of the reaction with Pd/C were 0%

had a positive effect on the selectivity of the reaction, due to the coarser structure of porous cobalt and the non-porous structure of Pd/C (Figs. S3–S5). Moreover, comparison between the two alloys revealed that CoPd was more active but less selective than Co₂Pd₃, meaning that they "obeyed" the reactivity-selectivity principle myth [36].

4. Conclusions

We introduced two Co-Pd bi-complex salts, namely [Co(NH₃)₆]₂[PdCl₄]₃·8 H₂O (**1**) and [Co(NH₃)₅Cl][PdCl₄] (**2**) as precursors for Co-Pd alloys. Applying hydrogen-mediated chemical reduction process on these BCS induced the formation of Co₂Pd₃ and CoPd nano-porous alloys with relatively high surface areas. Under the same process, cobalt complex salt and palladium complex salt induced the formation of porous cobalt and nano-porous palladium, respectively. These metallic materials preserved the morphologies of their micro-crystallites salt precursors. The alloys also preserved the stoichiometric Co/Pd ratio in their BCS precursors. The catalytic reactivity of these alloys was examined in hydrogenation of phenylacetylene, using DOE to optimize the conditions of the reaction. The reactivity of the alloys in the optimized conditions was compared with pure cobalt porous metal, pure palladium nano-porous metal and Pd/C reactivities. These experiments illustrated the utility of using DOE instead of "one variable at a time" method to reach the optimized conditions using only a few experiments. In addition, the presence of cobalt atoms within the alloys enabled their facile separation at the end of the reaction using a simple magnet. Moreover, the alloys showed improved catalytic properties compared to the pure metals and high yields towards styrene. Furthermore, based on our experiments, we suggest that nano-porous structure may improve the selectivity achieved by bimetallic alloy catalysts. Subsequently, further investigation of Co-Pd and other bimetallic nano-porous alloys catalytic and recycling properties may extend their applicability in other catalytic reactions or for energy storage.

CRedit authorship contribution statement

Shay Avisar: Synthesis, data analysis, Writing manuscript. **Yahel Shner:** Synthesis. **Raed Abu-Reziq:** Supervising catalytic processes. **Inna Popov:** Analytical procedures, Data interpretation. **Avi Bino:** Project coordinator.

Declaration of Competing Interest

The authors declare that they have no known competing financial interests or personal relationships that could have appeared to influence the work reported in this paper.

Acknowledgments

We are grateful to Dr. Benny Bogoslavsky and Dr. Shmuel Cohen for assistance with SC-XRD and PXRD analysis. We wish to thank Dr. Benny Bogoslavsky and Anat Shvets with proof reading of this article. We thank Atzmon Vakahi for his assistance with FIB tomography analysis. We also thank Dr. Vladimir Uvarov for structural characterization and theoretical support, and Suheir Omar for her assistance with preliminary catalytic experiments.

Appendix A. Supporting information

Supplementary data associated with this article can be found in the online version at doi:10.1016/j.jallcom.2021.161936.

References

- [1] M. Sankar, N. Dimitratos, P.J. Miedziak, P.P. Wells, C.J. Kiely, G.J. Hutchings, Designing bimetallic catalysts for a green and sustainable future, *Chem. Soc. Rev.* 41 (2012) 8099–8100, <https://doi.org/10.1039/c2cs35296f>
- [2] R. Ferrando, J. Jellinek, R.L. Johnston, Nanoalloys: from theory to applications of alloy clusters and nanoparticles, *Chem. Rev.* 108 (2008) 845–910, <https://doi.org/10.1021/cr040090g>
- [3] A.J. Forty, Corrosion micromorphology of noble metal alloys and depletion gilding, *Nature* 282 (1979) 597–598, <https://doi.org/10.1038/282597a0>
- [4] J. Erlebacher, M.J. Aziz, A. Karma, N. Dimitrov, K. Sieradzki, Evolution of nanoporosity in dealloying, *Nature* 410 (2001) 450–453, <https://doi.org/10.1038/35068529>
- [5] Y. Sun, Y. Xia, Mechanistic study on the replacement reaction between silver nanostructures and chloroauric acid in aqueous medium, *Am. Chem. Soc.* 126 (2004) 3892–3901, <https://doi.org/10.1021/ja039734c>
- [6] S.E. Skrabalak, J. Chen, Y. Sun, X. Lu, L. Au, C.M. Cobley, Y. Xia, Gold nanocages: synthesis, properties, and applications, *Acc. Chem. Res.* 41 (2008) 1587–1595, <https://doi.org/10.1021/ar800018v>
- [7] J.C. Thorp, K. Sieradzki, L. Tang, P.A. Crozier, A. Misra, M. Nastasi, D. Mitlin, S.T. Picraux, Formation of nanoporous noble metal thin films by electrochemical dealloying of PtSi_{1-x}, *Appl. Phys. Lett.* 88 (2006) 033110, <https://doi.org/10.1063/1.2161939>
- [8] X. Wang, Z. Qi, C. Zhao, W. Wang, Z. Zhang, Influence of alloy composition and dealloying solution on the formation and microstructure of monolithic nanoporous silver through chemical dealloying of Al-Ag alloys, *J. Phys. Chem. C* 113 (2009) 13139–13150, <https://doi.org/10.1021/jp902490u>
- [9] J. Weissmüller, R.C. Newman, H.-J. Jin, A.M. Hodge, J.W. Kysar, Nanoporous metals by alloy corrosion: formation and mechanical properties, *MRS Bull.* 34 (2009) 577–586, <https://doi.org/10.1557/mrs2009.157>
- [10] J. Yu, Y. Ding, C. Xu, A. Inoue, T. Sakurai, M. Chen, Nanoporous metals by dealloying multicomponent metallic glasses, *Chem. Mater.* 20 (2008) 4548–4550, <https://doi.org/10.1021/cm8009644>
- [11] H. Rösner, S. Parida, D. Kramer, C.A. Volkert, J. Weissmüller, Reconstructing a nanoporous metal in three dimensions: an electron tomography study of dealloyed gold leaf, *Adv. Eng. Mater.* 9 (2007) 535–541, <https://doi.org/10.1002/adem.200700063>
- [12] H. Li, A. Misra, J.K. Baldwin, S.T. Picraux, Synthesis and characterization of nanoporous Pt-Ni alloys, *Appl. Phys. Lett.* 95 (2009) 201902, <https://doi.org/10.1063/1.3265744>
- [13] Y.V. Shubin, S.V. Korenev, K.V. Yusenko, T.M. Korda, A.B. Venediktov, Powder X-ray diffraction study of the double complexes [M(NH₃)₅Cl][M'Cl₄] as precursors of metal powders (M = Ir, Rh, Co; M' = Pt, Pd), *Russ. Chem. Bull.* 51 (2002) 41–45, <https://doi.org/10.1023/A:1015045310216>
- [14] S.V. Korenev, A.B. Venediktov, Y.V. Shubin, S.A. Gromilov, K.V. Yusenko, Synthesis and structure of binary complexes of platinum group metals - Precursors of metallic materials, *J. Struct. Chem.* 44 (2003) 46–59, <https://doi.org/10.1023/A:1024980930337>
- [15] A. Zadesenets, E. Filatov, P. Plyusnin, I. Baidina, V. Dalezky, Y. Shubin, S. Korenev, A. Bogomyakov, Bimetallic single-source precursors [M(NH₃)₄][Co(C₂O₄)₂(H₂O)₂·2H₂O] (M = Pd, Pt) for the one run synthesis of CoPd and CoPt magnetic nanoalloys, *Polyhedron* 30 (2011) 1305–1312, <https://doi.org/10.1016/j.poly.2011.02.012>
- [16] M. Avisar-Levy, O. Levy, O. Ascarelli, I. Popov, A. Bino, Fractal structures of highly-porous metals and alloys at the nanoscale, *J. Alloy. Compd.* 635 (2015) 48–54, <https://doi.org/10.1016/j.jallcom.2015.02.073>
- [17] Y.V. Shubin, P.E. Plyusnin, S.V. Korenev, Determination of the equilibrium miscibility gap in the Pd - Rh alloy system using metal nanopowders obtained by decomposition of coordination compounds, *J. Alloy. Compd.* 622 (2015) 1055–1060, <https://doi.org/10.1016/j.jallcom.2014.10.187>
- [18] Y. Shubin, P. Plyusnin, M. Sharafutdinov, E. Makotchenko, S. Korenev, Successful synthesis and thermal stability of immiscible metal Au-Rh, Au-Ir and Au-Ir-Rh nanoalloys, *Nanotechnology* 28 (2017) 205302, <https://doi.org/10.1088/1361-6528/aa6bc9>
- [19] P.V. Snytnikov, K.V. Yusenko, S.V. Korenev, Y.V. Shubin, V.A. Sobyanyin, Co-Pt bimetallic catalysts for the selective oxidation of carbon monoxide in hydrogen-containing mixtures, *Kinet. Catal.* 48 (2007) 276–281, <https://doi.org/10.1134/S0023158407020127>
- [20] D.I. Potemkin, E.Y. Semitut, Y.V. Shubin, P.E. Plyusnin, P.V. Snytnikov, E.V. Makotchenko, D.Y. Osadchii, D.A. Svintsitskiy, S.A. Venyaminov, S.V. Korenev, V.A. Sobyanyin, Silica, alumina and ceria supported Au-Cu nanoparticles prepared via the decomposition of [Au(en)₂]₂[Cu(C₂O₄)₂]₃·8H₂O single-source precursor: synthesis, characterization and catalytic performance in CO PROX, *Catal. Today* 235 (2014) 103–111, <https://doi.org/10.1016/j.cattod.2014.04.026>
- [21] S. Nijem, S. Dery, M. Carmiel, G. Horesh, J. Garrevoet, K. Spiers, G. Falkenberg, C. Marini, E. Gross, Bimetallic Pt-Re nanoporous networks: synthesis, characterization, and catalytic reactivity, *J. Phys. Chem. C* 122 (2018) 24801–24808, <https://doi.org/10.1021/acs.jpcc.8b07863>
- [22] M. Carmiel-Kostan, S. Nijem, S. Dery, G. Horesh, E. Gross, Composition-reactivity correlations in platinum-cobalt nanoporous network as catalyst for hydrode-oxygenation of 5-hydroxymethylfurfural, *J. Phys. Chem. C* 123 (2019) 30274–30282, <https://doi.org/10.1021/acs.jpcc.9b07453>
- [23] R. Leardi, Experimental design in chemistry: a tutorial, *Anal. Chim. Acta* 652 (2009) 161–172, <https://doi.org/10.1016/j.jca.2009.06.015>

- [24] P.M. Murray, S.N.G. Tyler, J.D. Moseley, Beyond the numbers: charting chemical reaction space, *Org. Process Res. Dev.* 17 (2013) 40–46, <https://doi.org/10.1021/op300275p>
- [25] G.D. Bowden, B.J. Pichler, A. Maurer, A. Design, of experiments (DoE) approach accelerates the optimization of copper-mediated 18F-fluorination reactions of arylstannanes, *Sci. Rep.* 9 (2019) 1–10, <https://doi.org/10.1038/s41598-019-47846-6>
- [26] T.A. Shear, F. Lin, L.N. Zakharov, D.W. Johnson, "Design of experiments" as a method to optimize dynamic disulfide assemblies: cages and functionalizable, in: *Macrocycles, Chemie- Angew (Eds.), Int.* 59 2020, pp. 1496–1500, <https://doi.org/10.1002/anie.201912169>
- [27] H. Tye, M. Whittaker, Use of a design of experiments approach for the optimization of a microwave assisted Ugi reaction, *Org. Biomol. Chem.* 2 (2004) 813–815, <https://doi.org/10.1039/b400298a>
- [28] H. Tye, Application of statistical "design of experiments" methods in drug discovery, *Drug Discov. Today* 9 (2004) 485–491, [https://doi.org/10.1016/S1359-6446\(04\)03086-7](https://doi.org/10.1016/S1359-6446(04)03086-7)
- [29] A.F. Silva, P. Neves, S.M. Rocha, C.M. Silva, A.A. Valente, Optimization of continuous-flow heterogeneous catalytic oligomerization of 1-butene by design of experiments and response surface methodology, *Fuel* 259 (2020) 116256, <https://doi.org/10.1016/j.fuel.2019.116256>
- [30] SMART-NT V5.6, Bruker AXS GmbH, D-76181 Karlsruhe, Germany, 2002.
- [31] SAINT-NT V5.0, Bruker AXS GmbH, D-76181 Karlsruhe, Germany, 2002.
- [32] SHELXTL-NT V6.1, Bruker AXS GmbH, D-76181 Karlsruhe, Germany, 2002.
- [33] T.B. Massalski, H. Okamoto, P.R. Subramanian, L. Kacprzak (Eds.), *Binary Alloy Phase Diagrams, Second ed.*, ASM International, 1990.
- [34] J. Erlebacher, R. Seshadri, Hard materials with tunable porosity, *MRS Bull.* 34 (2009) 561–568, <https://doi.org/10.1557/mrs2009.155>
- [35] M. Ames, J. Markmann, R. Karos, A. Michels, A. Tschöpe, R. Birringer, Unraveling the nature of room temperature grain growth in nanocrystalline materials, *Acta Mater.* 56 (2008) 4255–4266, <https://doi.org/10.1016/j.actamat.2008.04.051>
- [36] H. Mayr, A.R. Ofial, The reactivity-selectivity principle: an imperishable myth in organic chemistry, *Angew. Chem. - Int. Ed.* 45 (2006) 1844–1854, <https://doi.org/10.1002/anie.200503273>